ACS APPLIED MATERIALS & INTERFACES

www.acsami.org

Research Article

A Light-Powered Triboelectric Nanogenerator Based on the Photothermal Marangoni Effect

Chongxian Liu, Dongjie Jiang, Guiqiang Zhu, Zengzhao Li, Xiaojie Zhang, Pan Tian, Dan Wang, Engui Wang, Han Ouyang,* Meng Xiao,* and Zhou Li*

Cite This: *ACS Appl. Mater. Interfaces* 2022, 14, 22206−22215

Read Online

ACCESS | Metrics & More | Article Recommendations | Supporting Information

ABSTRACT: The photothermal Marangoni effect enables direct light-to-work conversion, which is significant for realizing the self-propulsion of objects in a noncontact, controllable, and continuous manner. Many promising applications have been demonstrated in micro- and nanomachines, light-driven actuators, cargo transport, and gear transmission. Currently, the related studies about photothermal Marangoni effect-induced self-propulsion, especially rotational motions, remain focused on developing the novel photothermal materials, the structural designs, and the controllable self-propulsion modes. However, extending the related research from the laboratory practice to practical application remains a challenge. Herein, we combined the photothermal Marangoni effect-induced self-propulsion with the triboelectric nanogenerator technology for sunlight intensity determination. Photothermal black silicon, superhydrophobic copper foam with drag-reducing property, and triboelectric polytetrafluoroethylene film were integrated to fabricate a triboelectric nanogenerator. The photothermal-Marangoni-driven triboelectric nanogenerator (PMD-TENG) utilizes the photothermal Marangoni effect-induced self-propulsion to realize the relative motion between the triboelectric layer and the electrode, converting light into electrical signals, with a peak value of 2.35 V. The period of the output electrical signal has an excellent linear relationship with the light intensity. The accessible electrical signal generation strategy proposed here provides a new application for the photothermal Marangoni effect, which could further inspire the practical applications of the self-powered system based on the photothermal Marangoni effect, such as intelligent farming.

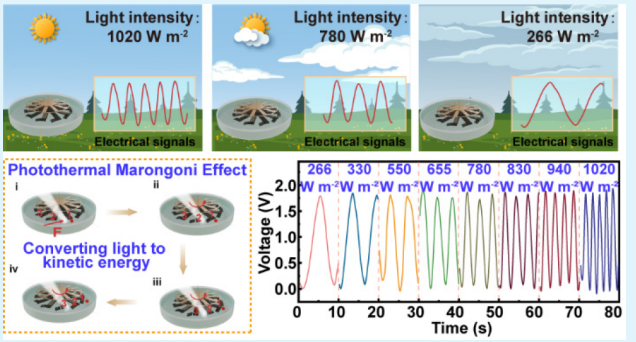

KEYWORDS: *photothermal Marangoni effect, self-powered, rotational motion, triboelectric nanogenerator, energy conversion*

INTRODUCTION

The Marangoni effect[1−3] refers to mass transfer along with the interface between two fluids due to the surface tension gradient and demonstrates promising applications in environmental remediation,[4] targeted drug delivery,[5] energy conversion,[6−8] self-assembly,[3,9] and so on. Because surface tension is sensitive to changes in temperature, temperature variation will lead to a surface tension gradient and the consequent fluid flow, which is called the thermal Marangoni effect.[10,11] The photothermal Marangoni effect is considered as an effective way for micro/macro-scale objects to realize the self-propulsion because the light, as ubiquitous and versatile energy, is transmitted in a remote, contactless, and accurate manner.[12−14] Under light irradiation, a local surface tension gradient can be generated around the objects and propel the objects to move, showing a simple unidirectional self-propulsion mode. Generally, given the application of motion, it requires not only self-propulsion ability but also controllability and programmability of the propulsion.

To our best knowledge, many efforts have been devoted to realizing multiple controllable self-propulsion modes of the objects. For example, linear and curvilinear motions[14] can be realized by focusing light on specific regions of the objects.[11,13−26] In this way, objects can be propelled across complicated routes, demonstrating promising applications, such as cargo delivery[16] and light-driven actuators.[25] Compared to the linear and curvilinear motions, rotational motions produced a cyclical and continuous mode. In such a mode, the mechanical energy performed a consistent and continuous output, which is advantageous for electrical signal generation. In general, two strategies have been developed to realize rotational motions.[12−14,16−20,22,23,27,28] First, light was used to irradiate local regions of cross-shaped photothermal materials.[18] Second, omnidirectional light was applied to irradiate the gear-shaped photothermal materials. A net torque

Received: March 15, 2022
Accepted: April 26, 2022
Published: May 6, 2022

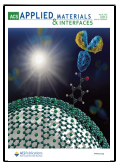

Downloaded via UNIV OF CHINESE ACADEMY OF SCIENCES on November 30, 2024 at 12:14:04 (UTC).
See https://pubs.acs.org/sharingguidelines for options on how to legitimately share published articles.

ACS Publications

© 2022 American Chemical Society

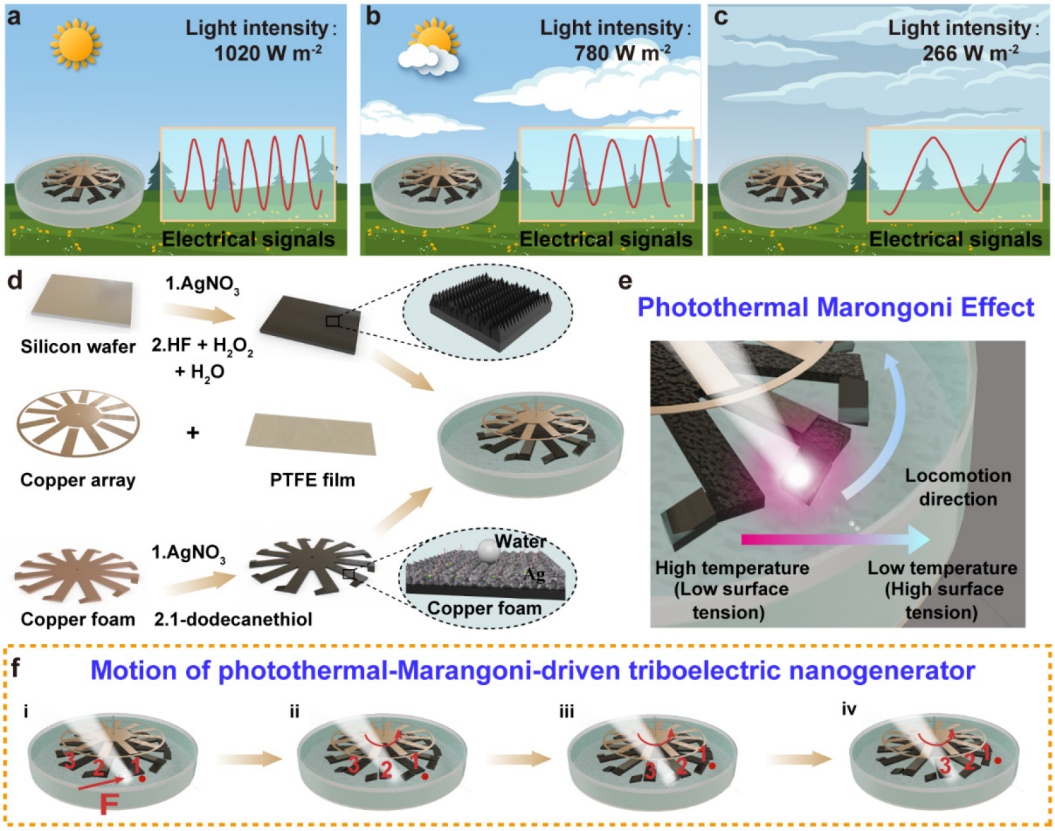

Figure 1. Schematic illustration showing the electrical signals generated by the photothermal-Marangoni-driven triboelectric nanogenerator (PMD-TENG) under sunlight light with different intensities: (a) 1020, (b) 780, and (c) 266 W m^{-2}. (d) Schematic illustration of the preparation process of the PMD-TENG. (e) Schematic illustration of the photothermal Marangoni effect mechanism. (f) Movement process of the rotator in the PMD-TENG under light irradiation.

can be generated by the nonuniform surface tension gradients to drive the object for rotation.[12] However, related studies on photothermal Marangoni effect-induced rotational motion are mainly restricted to fundamental aspects, such as the preparation of novel photothermal materials and the structural design. It remains a challenge to develop its practical applications.

Because the specially consistent and continuous output of rotational mechanical energy is advantageous for electrical characteristics,[29−48] herein, we designed a photothermal Marangoni-driven triboelectric nanogenerator (PMD-TENG), which utilizes black silicon to convert optical energy to thermal energy, inducing the photothermal Marangoni effect to propel the rotation of the rotator for the relative motion between the triboelectric layer and the electrode. The PMD-TENG generated an induced voltage with a peak value of 2.35 V. The system combined the photothermal Marangoni effect-induced rotational motion with the triboelectric nanogenerator technology, realizing the conversion from optical energy to electrical signals. Moreover, the frequency of the obtained electrical signals under light irradiation exhibited a computable relation with the optical information on the incident light. We envision that this work exploits a new application for the photothermal Marangoni effect-induced self-propulsion in electrical signal generation and inspires further exploration in energy conversion.

RESULTS AND DISCUSSION

Fabrication of the PMD-TENG. The designed PMD-TENG can convert light into distinguishable electrical signals under light irradiation with different intensities, as shown in Figure 1a−c. The fabrication process of PMD-TENG is schematically illustrated in Figure 1d. It mainly consists of a rotator and a stator. The rotator contains three parts: the black silicon as the photothermal material, the polytetrafluoroethylene (PTFE) films used as the triboelectric material, and the superhydrophobic copper foam to reduce fluidic drag during motion and load PTFE films. First, the black silicon was constructed by cutting the silicon wafer into a square with 5 × 5 mm^2 dimensions. Next, the square-shaped silicon wafers were subjected to chemical etching in $AgNO_3$(aq) and a mixed solution of $HF/H_2O_2/H_2O$ successively to obtain the silicon nanostructures (Figures S1 and S2, Supporting Information), with a visualized color change from silver to black. Second, PTFE films (10 mm in length, 5 mm in width, and 0.3 mm in thickness) were prepared by cutting a piece of PTFE film. Third, the superhydrophobic copper foam was manually fabricated by immersing copper foam (12 centrally connected units separated by equal degrees with an angle of 30°, as shown in Figure S3) in $AgNO_3$(aq) for the electroless deposition of silver aggregates and then immersing in an ethanol solution of 1-dodecanethiol overnight (Figures S4 and S5). The distance between two adjacent fins is crucial for the continuous rotational movement of the rotator. When black silicon is exposed to light, it will generate a driving force due to the photothermal Marangoni effect to propel the rotational part to

https://doi.org/10.1021/acsami.2c04651
ACS Appl. Mater. Interfaces 2022, 14, 22206−22215

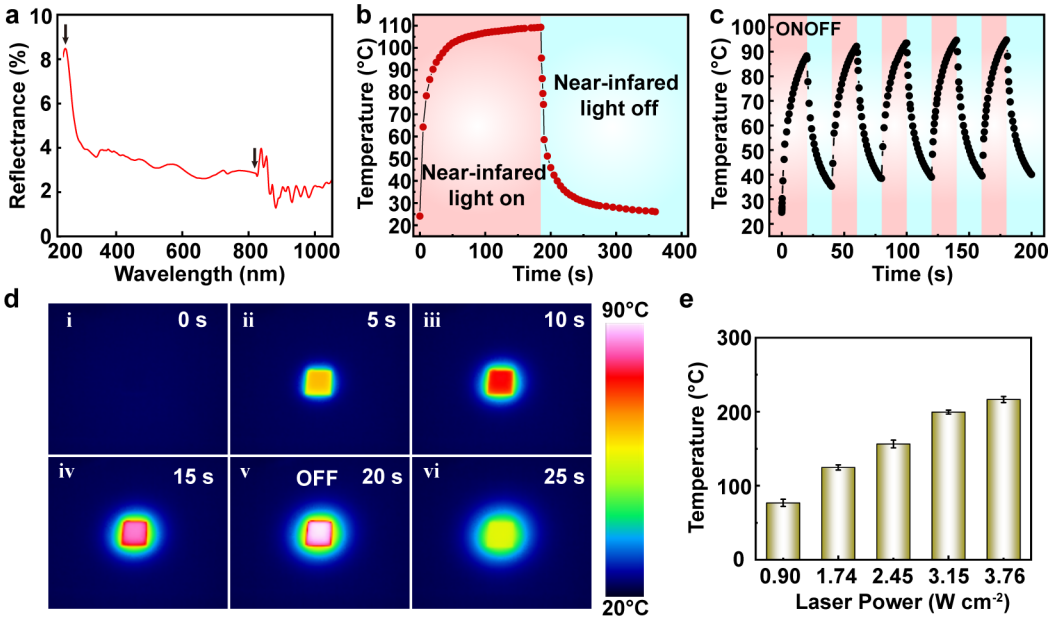

Figure 2. Characterization of the light absorption capabilities and the photothermal conversion properties of black silicon. (a) UV−vis reflection spectrum of black silicon. (b) Time-dependent surface temperature change of black silicon under near-infrared (NIR) light irradiation (808 nm, 0.9 W cm^{-2}). (c) Surface temperature change of black silicon during five heating/cooling cycles. (d) Infrared thermal imaging photos of black silicon under 808 nm NIR light irradiation (0.9 W cm^{-2}) during the light on/light off cycle. (e) Maximum temperature reached of black silicon under light irradiation with different light powers within 10 s.

rotate. After the former black silicon moves forward away from the irradiation area, the copper foam remains rotated because of the inertia force until the next black silicon is exposed to the light. Then the second black silicon generates the driving force to propel the rotator continuously and so on in a similar fashion. Therefore, the number of fins and the distance between adjacent fins are essential in determining whether the rotor can achieve a continuous rotational motion or not. If the distance between two adjacent fins is large, the inertial force generated by the former black silicon is not sufficient to make the rotator revolve continuously. Therefore, simultaneously given the minimum distance between two adjacent black silicons that afford the continuous rotation and the mass of the device that induces resistance during the motion, 12-fins was the optimal construction. Finally, the above three parts were assembled (Figure S6). In addition, the stator was fabricated by depositing two complementary-patterned Cu electrode networks through the printed circuit-board technology in a circular polyimide substrate (30 mm in diameter and 0.34 mm in thickness), as shown in Figure S7.

Rotational Motion of the PMD-TENG. The rotational motion mechanism of the PMD-TENG is schematically illustrated in Figure 1e. When the rotator is placed on the water surface, a thin air layer between the superhydrophobic copper foam and water exists to reduce the fluid drag. Moreover, an air gap (~2 mm) between the stator and the rotator is arranged. Moreover, we used a glass pillar through a hole in the superhydrophobic copper foam center to fix the location of the PMD-TENG when it was rotating on the water surface. Under light irradiation, the black silicon converts light to heat based on the photothermal effect, and then the generated heat is transmitted to the surrounding water, resulting in the temperature gradient and the consequent surface tension gradient. The surface tension gradient produces a Marangoni flow, propelling the macroscopic objects with a rotational mode.

Figure 1f displays the rotational motion process of the PMD-TENG under light irradiation. The state i, where black silicon #1 is exposed to light, is taken as the initial state. Based on the photothermal Marangoni effect, the driving force generated on black silicon #1 can make the rotator revolve counterclockwise (states i and ii). Although black silicon #1 moves far from the light, the rotator remains to rotate counterclockwise due to the inertia force until black silicon #2 is exposed to the light (state iii). Then, the black silicon #2 under light irradiation produces a propulsion force in the same way to make the rotator continue to rotate (states iii and iv). By that analogy, the counterclockwise rotational motion continued in this manner in the presence of light.

Characterization of the Photothermal Capacity of Black Silicon. The light absorption capacity was investigated by investigating the UV−vis absorption spectra of the as-prepared black silicon. As shown in Figure 2a, black silicon has a low reflectance of <10% at wavelengths of 220−1050 nm, demonstrating its high light absorption capability, which is of benefit to photothermal conversion. The peak at 226 nm is attributed to the porous nanostructures on the surface of black silicon. A jump of specular reflectance at ~827 nm is attributed to the change of grating in that range. To evaluate the photothermal property of black silicon, the surface temperature was monitored via an infrared thermal imaging camera, as shown in Figure 2b. When irradiated by 808 nm near-infrared (NIR) light with a power of 0.90 W cm^{-2}, the surface temperature of black silicon increased rapidly to 90 °C after 20 s of irradiation, demonstrating a rapid photothermal response, and then the temperature growth slowed and slowly increased to 109 °C. After removal of the NIR light, the surface temperature drops rapidly, showing that black silicon can quickly transfer heat to the surrounding medium. In addition,

https://doi.org/10.1021/acsami.2c04651
ACS Appl. Mater. Interfaces 2022, 14, 22206−22215

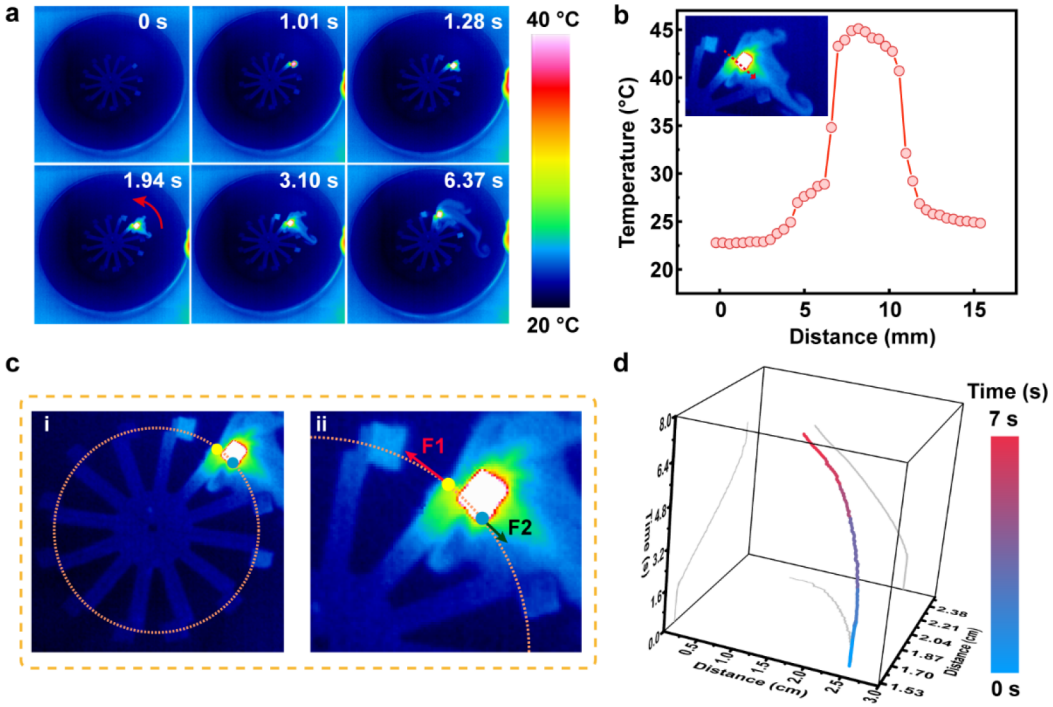

Figure 3. Movement of the rotational part in the TENG on the water surface. (a) Infrared thermal imaging photographs of the rotational part under 808 nm NIR light irradiation (3.76 W cm^{-2}). (b) Corresponding temperature distributions around the black silicon along the red line in the inset. The photograph is the infrared thermal imaging image at the beginning of the movement of the rotational part. (c) Thermography image (i) and surface tension analysis (ii) of the rotational part. (d) Counterclockwise rotational motion trajectory of the rotational part within 6 s.

to evaluate the stability of the photothermal property, the surface temperature was monitored during five light on/light off cycles (20 s/20 s). As shown in Figure 2c, the photothermal conversion ability of black silicon is well-maintained during five light on/light off cycles, indicating the stability of the light-to-heat conversion. As shown in Figure 2d, the surface temperature change of black silicon can be clearly observed by the thermal imaging images during the light on/light off cycle. Moreover, the photothermal conversion ability of black silicon was systematically investigated at different NIR light powers. With NIR light powers increasing from 0.90 to 3.76 W cm^{-2}, the maximum temperature increases from 75 to 216 °C within the same time interval (10 s), as shown in Figure 2e, suggesting that the photothermal property of black silicon could be well tuned by varying the light power. Thus, the above results indicate that black silicon has high light absorption capability and excellent photothermal conversion property.

Photothermal Conversion Ability of Black Silicon Floating on the Water Surface. Although exhibiting excellent photothermal properties in air, the photothermal conversion ability of black silicon on the water surface remains unclear, which is essential for the self-propulsion of the objects based on the photothermal Marangoni effect. After a superhydrophobic copper foam attached with black silicon (rotational part) was placed on the water surface, the 808 nm NIR light with a power of 3.76 W cm^{-2} was used to irradiate the black silicon. To clearly demonstrate the formed temperature gradient under light irradiation, the infrared thermal imaging photos of the black silicon were captured by an infrared thermal imaging camera within 6 s, as shown in Figure 3a and Video S1. Because of the excellent photothermal conversion property of black silicon, the surface temperature of black silicon rises rapidly, and the heat energy generated can be transferred to the superhydrophobic copper foam and water surface. To clearly demonstrate the motion mechanism of the rotational part, we further analyzed the thermal imaging image at the beginning of the movement. Figure 3b displays the temperature distribution along a red straight line in the inset of Figure 3b. According to the Harkins formula, the relationship between the surface tension of the fluid and temperature can be written as

$$e = b_0 + b_1 T + b_2 T^2 \quad (1)$$

where e denotes the surface tension, b_0, b_1, and b_2 are three constant terms (b_0 = 75.796 mN m^{-1}, b_1 = −0.145 mN m^{-1} $°C^{-1}$, b_2 = −0.00024 mN m^{-1} $°C^{-2}$), and T is the temperature of the fluid. On the basis of the formula, we find that the surface tension of the liquid has a negative relationship with its temperature. Generally, the force that drives the rotational part to revolve clockwise or counterclockwise needs to be perpendicular to the line between the center of the circle and the point of action. Thus, we compared two typical locations with the same radius around the rotational part (yellow dot and blue dot in Figure 3c(i)), where the infrared thermal imaging photographs in Figure 3c correspond to the photographs at 1.94 s in Figure 3a. As shown in Figure 3c(ii), the temperature of the yellow dot is much lower than that of the blue dot. The surface tension at the yellow dot is higher than that at the blue dot ($F1 > F2$), propelling the anticlockwise rotational motion of the rotational part. To clearly demonstrate the motion trajectory of the rotational part, its displacement at a different time under light irradiation is shown in Figure 3d. These results reveal that black silicon on water surfaces also exhibits excellent photothermal conversion properties, and the generated heat can be transmitted to the

https://doi.org/10.1021/acsami.2c04651
ACS Appl. Mater. Interfaces 2022, 14, 22206−22215

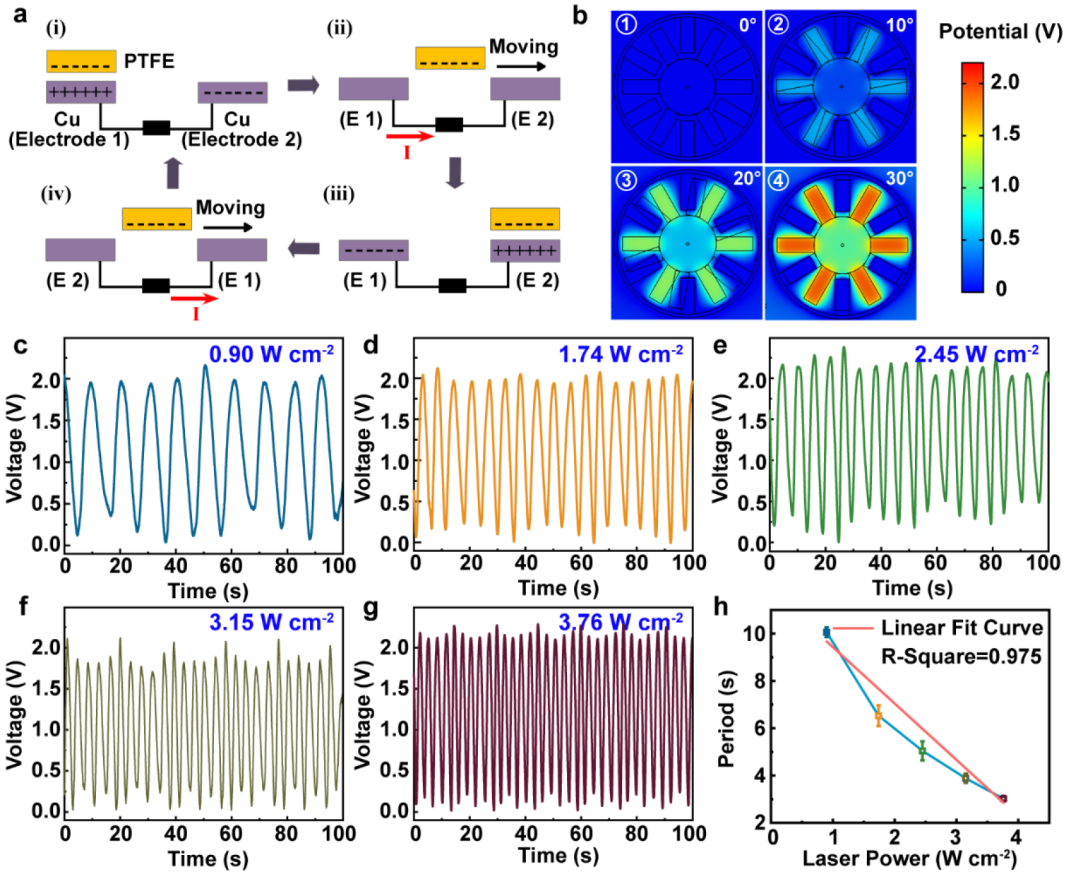

Figure 4. Working mechanism and output performance of the PMD-TENG under NIR light irradiation. (a) Schematic illustration of the working principle of the PMD-TENG under the relative rotational motion between the triboelectric layer (PTFE, yellow boxes) and Cu electrodes (gray boxes) in a typical cycle. (b) Simulation results of the electric potential distribution between the two complementary copper electrodes, which correspond to (i)−(iii) in (a). Voltage−time curves obtained under NIR light irradiation with a power of (c) 0.90, (d) 1.74, (e) 2.45, (f) 3.15, and (g) 3.76 W cm^{-2}. (h) Output frequency of induced electrical signals obtained under NIR light irradiation with different powers.

water surface to form a temperature gradient around the black silicon. Consequently, the temperature gradient can generate the surface tension gradient to produce fluid flows to realize the motion of the rotational part.[12,13]

Working Mechanism and Output Performance of the PMD-TENG under NIR Light Irradiation. After realizing the self-propulsion of the rotational part based on the photothermal Marangoni effect, we wondered whether we could utilize the self-propulsion of the rotational part to realize the relative motion between the triboelectric material and the electrode for electrical signal generation. The electrical signal-generating mechanism of the TENG is schematically described in Figure 4a. The process consists of two steps: the charging step on the PTFE films and the rotating electrostatic induction step. First, the PTFE film is charged by a corona needle with a polarization voltage of 10 kV for 15 min to load the PTFE film with negative charges. Second, the rotating electrostatic induction includes four steps in a typical cycle. When the PTFE film is placed exactly above Cu electrode 1 (E1), positive charges are induced on Cu electrode 1 due to electrostatic induction (state i). As the PTFE film revolves from E1 to Cu electrode 2 (E2) (states i and ii), the free electrons transfer from E2 to E1 by the external circuit to redistribute the charges on both electrodes. Until the PTFE film completely overlaps the right electrode, a large amount of positive charge is generated on E2. The PTFE film continues to rotate to the next segment of E1. The free electrons transfer back from E1 to E2, generating a current from E2 to E1. This is the electrical signal generation cycle of the TENG. In addition, we define the potential difference between the two electrodes (U_1, U_2) as the open-circuit voltage (V_{OC}) in the circuit ($V_{OC} = U_1 - U_2$). To visualize the continuous change in the open-circuit voltage, we calculated the electric potential distribution in different motion states by utilizing COMSOL Multiphysics simulation software (Figure 4b). Furthermore, the electrical-signal-generating ability of the TENG under NIR light with different powers was systematically investigated, as shown in Figure 4c−g. With the NIR laser light power increasing from 0.90 to 3.76 W cm^{-2}, the output frequency of the open-circuit voltage gradually increases from 0.1 to 0.33 Hz (Figure 4h). This result indicates that black silicon under light irradiation with higher power can produce a higher rotation velocity of the triboelectric layer, thereby significantly increasing the output frequency of induced electrical signals. In addition, the increase in the rotation velocity cannot change the peak electrical signals because there is no correlation between the peak electrical signals and the rotational velocity, as reported in a previous study.[43] According to the reported theoretical study of free-standing triboelectric nanogenerators, the voltage and the current are determined by the transferred charges.[49] Thus, we can increase the amount of transferred charges to increase the electrical output. There are two potential strategies to realize the purpose of further improvement of transferred charges from the reported devices. (1) The first strategy is to

https://doi.org/10.1021/acsami.2c04651
ACS Appl. Mater. Interfaces 2022, 14, 22206−22215

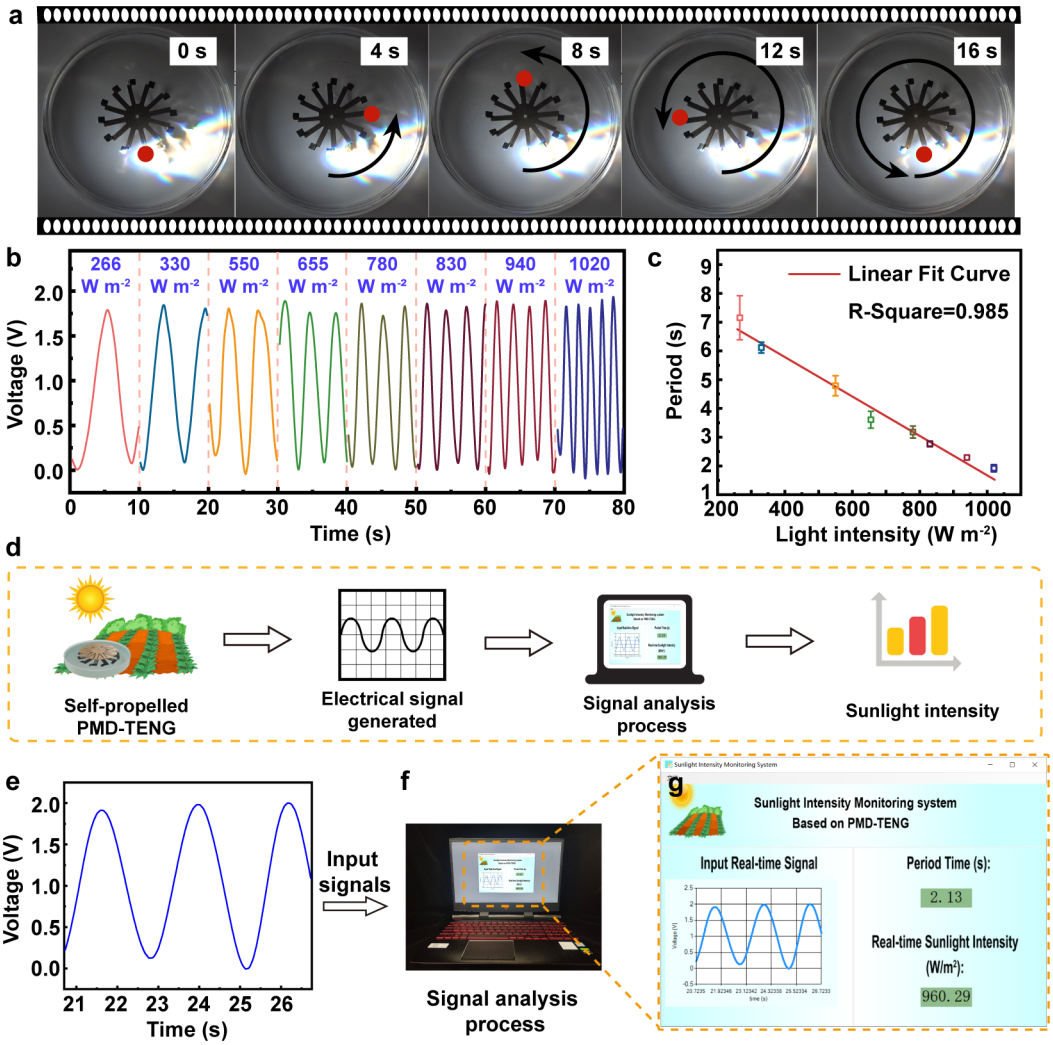

Figure 5. Application in sunlight intensity monitoring system. (a) Sunlight-induced rotational motions of the rotational part in the TENG. (b) Voltage−time curves obtained under sunlight irradiation with different powers of 266−1020 W m^{-2}. (c) Relationship between the induced electrical signal period with the sunlight intensity. (d) Fundamental process of the sunlight intensity monitoring system. (e) Electrical signal generated by the PMD-TENG under a certain sunlight intensity. (f) Photograph of the computer software analyzing the electrical signals, providing the (g) sunlight intensity information.

increase the size of the light-powered triboelectric nanogenerator. The increase in device size means that the area of triboelectric material can be increased, which could increase the transferred charges during the motion process. However, the increase in device size also means that the continuous rotational motion of the device requires a larger driving force generated by black silicon based on the photothermal Marangoni effect. To conduct this strategy, we can prepare black silicon with lower reflectivity by nanolithography and energetic beam etching techniques to improve the photothermal conversion efficiency, resulting in a larger temperature/surface tension gradient to propel the rotator with a large size. (2) The second strategy is to prepare negative triboelectric materials with surface microstructures. We can fabricate micro-/nanostructures on the surface of triboelectric materials (PTFE films) through microfabrication techniques and reactive ion etching techniques. These micro-/nanostructures can effectively increase the specific surface area and enhance the charge capture capability, thus improving the electrical output of the light-powered triboelectric nanogenerator. These results demonstrate that the rotational part based on the photothermal Marangoni effect can convert NIR light into kinetic energy to propel the triboelectric layers and the resultant relative motion with the electrode, leading to electrical signal generation (Figure S8).

Applications of the PMD-TENG in Sunlight Intensity Monitoring. Although we have confirmed that the NIR light energy can be harvested and converted into electrical signals by the PMD-TENG, whether the PMD-TENG can harvest the natural energy resource, e. g., sunlight, into electrical signals remains to be confirmed. The rotational part is exposed to sunlight (in June, Beijing) focused with a Fresnel lens (diameter: 300 mm; focal length: 260 mm). Figure 5a exhibits the counterclockwise rotational motion of the rotational part within 16 s (as recorded in Videos S2), demonstrating that black silicon can convert sunlight into heat to propel the superhydrophobic foam to rotate, which is realized through the photothermal Marangoni effect. When the rotational part is applied to drive the triboelectric layers (PTFE films) to move, electric signals are generated. As shown in Figure 5b, as the sunlight intensity increases from 266 to 1020 W m^{-2}, the output frequency of the induced electrical signals increases.

https://doi.org/10.1021/acsami.2c04651
ACS Appl. Mater. Interfaces 2022, 14, 22206−22215

These results demonstrate that the temperature gradient induced by black silicon increases with increasing light intensity at the same time interval, resulting in a more significant driving force and a rotation velocity. Obviously, with the increase in the rotational velocity, the period of the induced electrical signals decreases from 7.9 to 1.9 s, as shown in Figure 5c. The coefficient of determination (R^2) between the period and the sunlight intensity reaches 0.985, exhibiting an excellent linear relationship. The excellent linear relationship demonstrates that the PMD-TENG may be used as an excellent sensor to monitor the sunlight intensity from 266 to 1020 W m^{-2}.

As a proof-of-concept potential application, we designed a sunlight intensity monitoring system based on the PMD-TENG, as shown in Figure 5d. The natural sunlight is first harvested and converted into electrical signals by the PMD-TENG. The electrical signals can be further analyzed in computer software. In this way, the period of the electrical signals was calculated into the sunlight intensity based on the linear relationship obtained above, providing the sunlight intensity information. Figure 5e displays the electrical signal under a certain sunlight intensity, and then the electrical signal is transmitted to the sunlight intensity monitoring software on the computer (Figure 5f). Finally, the intensity of the incident sunlight can be obtained (Figure 5g). Thus, the natural energy, e.g., sunlight, can be harvested and converted into electrical signals by the PMD-TENG.

EXPERIMENTAL SECTION

Chemicals. The following chemicals were used as supplied. Ethanol, H_2SO_4, H_2O_2, KOH, and isopropyl alcohol were purchased from Beijing Chemical Works. $AgNO_3$ and HF were obtained from Sinopharm Chemical Reagent Co., Ltd. 1-Dodecanethiol was purchased from Aladdin Reagent Co., Ltd., China. The copper foam (0.8 mm in thickness) was purchased from Kunshan Jiayisheng Electronics Co., Ltd. The polished silicon wafer was obtained from Suzhou Crystal Silicon Electronic & Technology Co., Ltd. The polytetrafluoroethylene (0.18 mm in thickness) film was purchased from Hubei Aikel Engineering Plastic Co., Ltd.

Characterization and Measurement. A solarimeter (SM206) from the Shenzhen Xinbaorui Instruments Company was used to measure the intensity of natural sunlight. The Fresnel lenses were purchased from Shenzhen Yingmei Scientific Co., Ltd. The 940 nm NIR laser source was purchased from Beijing Laserwave Optoelectronics Tech. Co., Ltd. The voltage−time curves are measured by an electrometer (Keithley 6517 System) and recorded by an oscilloscope (Teledyne LeCroy HD 4096). Scanning electron microscopy (Zeiss EVO MA25, 20 kV) measurements were performed to investigate the morphology and structure of all samples. Water contact angle measurements were taken with a contact angle system (DataPhysics-OCA20). The reflection properties of the black silicon were measured by using a UV−vis spectrophotometer (UV-3900).

Fabrication of the Superhydrophobic Copper Foam. First, a piece of copper foam was cut into 12 centrally connected units separated by equal degrees with an angle of 30°. Second, the copper foam was ultrasonically cleaned alternately in ethanol, an ethanol/water solution (v/v, 1:1), and water for 5 min, successively. Third, the above copper foam was immersed in an aqueous solution of $AgNO_3$ (0.02 M) for electroless deposition for 15 min, washed with water, and dried in an oven. Finally, the foamed copper was immersed in an ethanol solution of 1-dodecanethiol (1 mM) for 12 h, washed with absolute ethanol, and dried in an oven.

Fabrication of Black Silicon. First, the silicon wafer was cleaned in a mixed solution of H_2SO_4 and H_2O_2 (v/v, 7:3) for 30 min, washed with water, and dried with nitrogen flow. Second, the cleaned silicon wafer was immersed in a mixture solution of 3 wt % potassium hydroxide and 8 vol % isopropanol at 80 °C for 30 min and washed with deionized water. Third, the above silicon wafer was immersed in an aqueous solution of $AgNO_3$ (0.008 M) for 3 min and then immersed in a mixed solution of HF, H_2O_2, and H_2O (v/v/v, 2:1:10) for 7 min. Finally, the silicon wafer was immersed in nitric acid to remove the residual silver particles. The substrate showed a visualized color change from silver to black.

Water Contact Angle Measurements. A droplet of 4 μL of deionized water was used for measurements, and an optical contact angle system was used to record the static water contact angle and sliding angle of the sample. An average of five measurements at different sites on the sample were measured.

Maximum Temperature of Black Silicon under Different Light Intensities. Black silicon (5 × 5 cm^2) was placed below the light source at 3 cm. The temperature change of black silicon during the same time interval (10 s) under different light intensities (808 nm) was monitored and recorded by an IR camera. Afterward, we analyzed the temperature on the software through fixing a frame that was smaller than the black silicon, and the maximum temperature in the frame at the point of 10 s irradiation was recorded. Finally, the results of repeated experiments were collected for the statistics analysis.

CONCLUSIONS

In summary, we combined the photothermal Marangoni effect-induced self-propulsion with the triboelectric nanogenerator technology to realize the monitoring of natural energy. A photothermal-Marangoni-driven triboelectric nanogenerator (PMD-TENG) was fabricated, which utilizes the photothermal Marangoni effect-induced self-propulsion of black silicon to realize the relative motion between the triboelectric layer and the electrode. The black silicon exhibited high light absorption capacity and excellent photothermal conversion property. While the rotator of the PMD-TENG floats on the water surface, the black silicon can convert the light into heat power to drive the rotator to rotate. The relative rotational motion between the rotator and the stator of the TENG can generate an open circuit voltage of 2.35 V. Moreover, there is an excellent linear relationship between the period of the electrical signals and the sunlight intensity. We believe that this study extends the application of self-propelled objects based on the photothermal Marangoni effect and inspires the development of related research from laboratory practice to practical applications.

ASSOCIATED CONTENT

Supporting Information

The Supporting Information is available free of charge at https://pubs.acs.org/doi/10.1021/acsami.2c04651.

SEM images of the untreated silicon wafer and the silicon wafer after chemical etching (Figure S1); atomic force microscope (AFM) images the untreated silicon wafer and the silicon wafer after chemical etching and corresponding sectional analyses of the untreated silicon wafer and the silicon wafer after chemical etching (Figure S2); schematic illustration of dimensions of the superhydrophobic copper foam (Figure S3); SEM images of the copper foam before and after electroless metal deposition, EDS patterns of the untreated copper foam, and copper foam deposited with silver aggregates before and after modification by the low-surface-energy coating, and water contact angle (WCA) of the as-prepared superhydrophobic surface (Figure S4); optical photograph of sliding angle of the superhydrophobic copper foam (Figure S5); optical photograph after

https://doi.org/10.1021/acsami.2c04651
ACS Appl. Mater. Interfaces 2022, 14, 22206−22215

assembling the superhydrophobic copper foam, the black silicon, and the polytetrafluoroethylene films (Figure S6); optical photograph of the stator (the copper electrode) of the photothermal-Marangoni-driven triboelectric nanogenerator (PMD-TENG) (Figure S7); voltage−time curves and transfer charge−time curves obtained under NIR light irradiation with power of 3.76 W cm^{-2} (Figure S8) (PDF)
Video S1 (MP4)
Video S2 (MP4)

AUTHOR INFORMATION

Corresponding Authors

Meng Xiao − *Key Laboratory of Radiopharmacokinetics for Innovative Drugs, Chinese Academy of Medical Sciences, and Institute of Radiation Medicine, Chinese Academy of Medical Sciences & Peking Union Medical College, Tianjin 300192, People's Republic of China*; Email: xiaomeng@irm-cams.ac.cn

Han Ouyang − *School of Nanoscience and Technology, University of Chinese Academy of Sciences, Beijing 100049, People's Republic of China*; Email: ouyanghan@ucas.ac.cn

Zhou Li − *CAS Center for Excellence in Nanoscience, Beijing Key Laboratory of Micro-nano Energy and Sensor, Beijing Institute of Nanoenergy and Nanosystems, Chinese Academy of Sciences, Beijing 101400, People's Republic of China; School of Nanoscience and Technology, University of Chinese Academy of Sciences, Beijing 100049, People's Republic of China; Center on Nanoenergy Research School of Physical Science and Technology, Guangxi University, Nanning 530004, People's Republic of China*; orcid.org/0000-0002-9952-7296; Email: zli@binn.cas.cn

Authors

Chongxian Liu − *State Key Laboratory of Chemical Resource Engineering, Beijing University of Chemical Technology, Beijing 100029, People's Republic of China*; orcid.org/0000-0001-5162-4137

Dongjie Jiang − *CAS Center for Excellence in Nanoscience, Beijing Key Laboratory of Micro-nano Energy and Sensor, Beijing Institute of Nanoenergy and Nanosystems, Chinese Academy of Sciences, Beijing 101400, People's Republic of China; School of Nanoscience and Technology, University of Chinese Academy of Sciences, Beijing 100049, People's Republic of China*

Guiqiang Zhu − *State Key Laboratory of Chemical Resource Engineering, Beijing University of Chemical Technology, Beijing 100029, People's Republic of China*

Zengzhao Li − *State Key Laboratory of Chemical Resource Engineering, Beijing University of Chemical Technology, Beijing 100029, People's Republic of China*

Xiaojie Zhang − *State Key Laboratory of Chemical Resource Engineering, Beijing University of Chemical Technology, Beijing 100029, People's Republic of China*

Pan Tian − *State Key Laboratory of Chemical Resource Engineering, Beijing University of Chemical Technology, Beijing 100029, People's Republic of China*

Dan Wang − *State Key Laboratory of Chemical Resource Engineering, Beijing University of Chemical Technology, Beijing 100029, People's Republic of China*

Engui Wang − *Center on Nanoenergy Research School of Physical Science and Technology, Guangxi University, Nanning 530004, People's Republic of China*

Complete contact information is available at: https://pubs.acs.org/10.1021/acsami.2c04651

Author Contributions

C.L. and D.J. contributed equally to this work. Z.L., M.X., and H.O. supervised the project. C.L. and D.J. conceived the idea and designed the experiments. C.L., G.Z., Z.L., and X.Z. fabricated the devices and performed the characterizations of black silicon. C.L., P.T., and D.W. accomplished the graphs in the manuscript. C.L. and D.J. accomplished the electrical characterization. C.L. and E.W. performed the SEM characterizations of superhydrophobic copper foam. C.L., D.J., and M.X. wrote the manuscript. All authors reviewed and commented on the manuscript.

Notes

The authors declare no competing financial interest.

ACKNOWLEDGMENTS

Z.L. received funding from the National Natural Science Foundation of China (61875015, T2125003, 52003299, and 62004010), the Beijing Natural Science Foundation (JQ20038, L212010), and the Strategic Priority Research Program of the Chinese Academy of Sciences (XDA16021101). H.O. received funding from the National Natural Science Foundation of China (62004010). M.X. received funding from the National Natural Science Foundation of China (52003299).

REFERENCES

(1) Scriven, L. E.; Sternling, C. V. The Marangoni Effects. *Nature* **1960**, *187*, 186−188.
(2) Xiao, M.; Cheng, M.; Zhang, Y.; Shi, F. Combining the Marangoni Effect and the pH-Responsive Superhydrophobicity-Superhydrophilicity Transition to Biomimic the Locomotion Process of the Beetles of Genus Stenus. *Small* **2013**, *9*, 2509−2514.
(3) Xiao, M.; Xian, Y.; Shi, F. Precise Macroscopic Supramolecular Assembly by Combining Spontaneous Locomotion Driven by the Marangoni Effect and Molecular Recognition. *Angew. Chem., Int. Ed.* **2015**, *127*, 9080−9084.
(4) Kong, L.; Ambrosi, A.; Nasir, M. Z. M.; Guan, J.; Pumera, M. Self-Propelled 3D-Printed "Aircraft Carrier" of Light-Powered Smart Micromachines for Large-Volume Nitroaromatic Explosives Removal. *Adv. Funct. Mater.* **2019**, *29*, 1903872.
(5) Hsieh, M.-H.; Wei, H.-J.; Chen, K.-H.; Wang, H.-C.; Yu, C.-H.; Lu, T.-H.; Chang, Y.; Sung, H.-W. A Fast and Facile Platform for Fabricating Phase-Change Materials-Based Drug Carriers Powered by Chemical Marangoni Effect. *Biomaterials* **2021**, *271*, 120748.
(6) Cheng, M.; Zhang, D.; Zhang, S.; Wang, Z.; Shi, F. Tackling the Short-Lived Marangoni Motion Using a Supramolecular Strategy. *CCS Chem.* **2019**, *1*, 148−155.
(7) Frenkel, M.; Vilk, A.; Legchenkova, I.; Shoval, S.; Bormashenko, E. Mini-Generator of Electrical Power Exploiting the Marangoni Flow Inspired Self-Propulsion. *ACS Omega* **2019**, *4*, 15265−15268.
(8) Ikezoe, Y.; Fang, J.; Wasik, T. L.; Uemura, T.; Zheng, Y.; Kitagawa, S.; Matsui, H. Peptide Assembly-Driven Metal-Organic Framework (MOF) Motors for Micro Electric Generators. *Adv. Mater.* **2015**, *27*, 288−291.
(9) Cheng, M.; Zhu, G.; Li, L.; Zhang, S.; Zhang, D.; Kuehne, A. J. C.; Shi, F. Parallel and Precise Macroscopic Supramolecular Assembly through Prolonged Marangoni Motion. *Angew. Chem., Int. Ed.* **2018**, *57*, 14106−14110.
(10) Gugliotti, M.; Baptista, M. S.; Politi, M. J.; Silverstein, T. P.; Slater, C. D. Surface Tension Gradients Induced by Temperature: The Thermal Marangoni Effect. *J. Chem. Educ.* **2004**, *81*, 824−826.
(11) Xuan, H.; Guan, Q.; Zhang, L.; You, Z. Thermoplastic Photoheating Polymer Enables 3D-Printed Self-Healing Light-Propelled Smart Devices. *Adv. Funct. Mater.* **2021**, *31*, 2009568.

(12) Wang, W.; Liu, Y.-Q.; Liu, Y.; Han, B.; Wang, H.; Han, D.-D.; Wang, J.-N.; Zhang, Y.-L.; Sun, H.-B. Direct Laser Writing of Superhydrophobic PDMS Elastomers for Controllable Manipulation via Marangoni Effect. *Adv. Funct. Mater.* **2017**, *27*, 1702946.
(13) Wang, W.; Han, B.; Zhang, Y.; Li, Q.; Zhang, Y. L.; Han, D. D.; Sun, H. B. Laser-Induced Graphene Tapes as Origami and Stick-On Labels for Photothermal Manipulation via Marangoni Effect. *Adv. Funct. Mater.* **2021**, *31*, 2006179.
(14) Hou, K.; Guan, D.; Li, H.; Sun, Y.; Long, Y.; Song, K. Programmable Light-Driven Swimming Actuators via Wavelength Signal Switching. *Sci. Adv.* **2021**, *7*, No. eabh3051.
(15) Okawa, D.; Pastine, S. J.; Zettl, A.; Fréchet, J. M. J. Surface Tension Mediated Conversion of Light to Work. *J. Am. Chem. Soc.* **2009**, *131*, 5396−5398.
(16) Liao, M.; Sun, H.; Tao, X.; Xu, X.; Li, Z.; Fu, X.; Xie, S.; Ye, L.; Zhang, Y.; Wang, B.; Sun, X.; Peng, H. The Alignment of Thermally Conducting Nanotubes Making High-Performance Light-Driving Motors. *ACS Appl. Mater. Interfaces* **2018**, *10*, 26765−26771.
(17) Su, X.; Li, H.; Lai, X.; Yang, Z.; Chen, Z.; Wu, W.; Zeng, X. Vacuum-Assisted Layer-By-Layer Superhydrophobic Carbon Nanotube Films with Electrothermal and Photothermal Effects for Deicing and Controllable Manipulation. *J. Mater. Chem. A* **2018**, *6*, 16910−16919.
(18) Yang, R.-L.; Zhu, Y.-J.; Qin, D.-D.; Xiong, Z.-C. Light-Operated Dual-Mode Propulsion at the Liquid/Air Interface Using Flexible, Superhydrophobic, and Thermally Stable Photothermal Paper. *ACS Appl. Mater. Interfaces* **2020**, *12*, 1339−1347.
(19) Yang, R.-L.; Zhu, Y.-J.; Chen, F.-F.; Qin, D.-D.; Xiong, Z.-C. Superhydrophobic Photothermal Paper Based on Ultralong Hydroxyapatite Nanowires for Controllable Light-Driven Self-Propelled Motion. *ACS Sustainable Chem. Eng.* **2019**, *7*, 13226−13235.
(20) Cao, W.-T.; Feng, W.; Jiang, Y.-Y.; Ma, C.; Zhou, Z.-F.; Ma, M.-G.; Chen, Y.; Chen, F. Two-Dimensional MXene-Reinforced Robust Surface Superhydrophobicity with Self-Cleaning and Photothermal-Actuating Binary Effects. *Mater. Horiz.* **2019**, *6*, 1057−1065.
(21) Zhou, X.; Li, Z.; Tan, L.; Zhang, Y.; Jiao, Y. Near-Infrared Light-Steered Graphene Aerogel Micromotor with High Speed and Precise Navigation for Active Transport and Microassembly. *ACS Appl. Mater. Interfaces* **2020**, *12*, 23134−23144.
(22) Wang, Y.; Dong, Y.; Ji, F.; Zhu, J.; Ma, P.; Su, H.; Chen, P.; Feng, X.; Du, W.; Liu, B.-F. Patterning Candle Soot for Light-Driven Actuator via Marangoni Effect. *Sensors Actuators B: Chem.* **2021**, *347*, 130613.
(23) Wang, X.; Dai, L.; Jiao, N.; Tung, S.; Liu, L. Superhydrophobic Photothermal Graphene Composites and their Functional Applications in Microrobots Swimming at the Air/Water Interface. *Chem. Eng. J.* **2021**, *422*, 129394.
(24) Wu, H.; Luo, J.; Huang, X.; Wang, L.; Guo, Z.; Liang, J.; Zhang, S.; Xue, H.; Gao, J. Superhydrophobic, Mechanically Durable Coatings for Controllable Light and Magnetism Driven Actuators. *J. Colloid Interface Sci.* **2021**, *603*, 282−290.
(25) Pan, D.; Wu, D.; Li, P. J.; Ji, S. Y.; Nie, X.; Fan, S. Y.; Chen, G. Y.; Zhang, C. C.; Xin, C.; Xu, B.; Zhu, S.; Cai, Z.; Hu, Y.; Li, J.; Chu, J. Transparent Light-Driven Hydrogel Actuator Based on Photothermal Marangoni Effect and Buoyancy Flow for Three-Dimensional Motion. *Adv. Funct. Mater.* **2021**, *31*, 2009386.
(26) Jian, Y.; Wu, B.; Yang, X.; Peng, Y.; Zhang, D.; Yang, Y.; Qiu, H.; Lu, H.; Zhang, J.; Chen, T. Stimuli-Responsive Hydrogel Sponge for Ultrafast Responsive Actuator. *Supramol. Mater.* **2022**, *1*, 100002.
(27) Yang, M.; Ripoll, M. A Self-Propelled Thermophoretic Microgear. *Soft Matter* **2014**, *10*, 1006−1011.
(28) Maggi, C.; Saglimbeni, F.; Dipalo, M.; De Angelis, F.; Di Leonardo, R. Micromotors with Asymmetric Shape that Efficiently Convert Light into Work by Thermocapillary Effects. *Nat. Commun.* **2015**, *6*, 7855.
(29) Yong, S.; Wang, J.; Yang, L.; Wang, H.; Luo, H.; Liao, R.; Wang, Z. L. Auto-Switching Self-Powered System for Efficient Broad-Band Wind Energy Harvesting Based on Dual-Rotation Shaft Triboelectric Nanogenerator. *Adv. Energy Mater.* **2021**, *11*, 2101194.
(30) Han, J.; Feng, Y.; Chen, P.; Liang, X.; Pang, H.; Jiang, T.; Wang, Z. L. Wind-Driven Soft-Contact Rotary Triboelectric Nanogenerator Based on Rabbit Fur with High Performance and Durability for Smart Farming. *Adv. Funct. Mater.* **2022**, *32*, 2108580.
(31) Rahman, M. T.; Rana, S. M. S.; Maharjan, P.; Salauddin, M.; Bhatta, T.; Cho, H.; Park, C.; Park, J. Y. Ultra-Robust and Broadband Rotary Hybridized Nanogenerator for Self-Sustained Smart-Farming Applications. *Nano Energy* **2021**, *85*, 105974.
(32) Bao, Y.; Wang, R.; Lu, Y.; Wu, W. Lignin Biopolymer Based Triboelectric Nanogenerators. *APL Mater.* **2017**, *5*, 074109.
(33) Suo, G.; Yu, Y.; Zhang, Z.; Wang, S.; Zhao, P.; Li, J.; Wang, X. Piezoelectric and Triboelectric Dual Effects in Mechanical-Energy Harvesting Using BaTiO3/Polydimethylsiloxane Composite Film. *ACS Appl. Mater. Interfaces* **2016**, *8*, 34335−34341.
(34) Zhang, Q.; Jin, T.; Cai, J. G.; Xu, L.; He, T. Y. Y.; Wang, T. H.; Tian, Y. Z.; Li, L.; Peng, Y.; Lee, C. K. Wearable Triboelectric Sensors Enabled Gait Analysis and Waist Motion Capture for IoT-Based Smart Healthcare Applications. *Adv. Sci.* **2022**, *9*, 2103694.
(35) Oh, H.; Kwak, S. S.; Kim, B.; Han, E.; Lim, G. H.; Kim, S. W.; Lim, B. Highly Conductive Ferroelectric Cellulose Composite Papers for Efficient Triboelectric Nanogenerators. *Adv. Funct. Mater.* **2019**, *29*, 1904066.
(36) Chen, C.; Wen, Z.; Shi, J.; Jian, X.; Li, P.; Yeow, J. T. W.; Sun, X. Micro Triboelectric Ultrasonic Device for Acoustic Energy Transfer and Signal Communication. *Nat. Commun.* **2020**, *11*, 4143.
(37) Yang, H.; Fan, F. R.; Xi, Y.; Wu, W. Design and Engineering of High-Performance Triboelectric Nanogenerator for Ubiquitous Unattended Devices. *EcoMat* **2021**, *3*, No. e12093.
(38) Deng, H. T.; Zhang, X. R.; Wang, Z. Y.; Wen, D. L.; Ba, Y. Y.; Kim, B.; Han, M. D.; Zhang, H. X.; Zhang, X. S. Super-Stretchable Multi-Sensing Triboelectric Nanogenerator Based on Liquid Conductive Composite. *Nano Energy* **2021**, *83*, 105823.
(39) Liu, L.; Shi, Q. F.; Sun, Z. D.; Lee, C. K. Magnetic-Interaction Assisted Hybridized Triboelectric-Electromagnetic Nanogenerator For Advanced Human-Machine Interfaces. *Nano Energy* **2021**, *86*, 106154.
(40) Rawy, K.; Sharma, R.; Yoon, H.-J.; Khan, U.; Kim, S.-W.; Kim, T. T.-H. A Triboelectric Nanogenerator Energy Harvesting System Based on Load-Aware Control for Input Power from 2.4 μW to 15.6 μW. *Nano Energy* **2020**, *74*, 104839.
(41) Zhang, N.; Qin, C.; Feng, T.; Li, J.; Yang, Z.; Sun, X.; Liang, E.; Mao, Y.; Wang, X. Non-Contact Cylindrical Rotating Triboelectric Nanogenerator for Harvesting Kinetic Energy From Hydraulics. *Nano Res.* **2020**, *13*, 1903−1907.
(42) Zhai, N.; Wen, Z.; Chen, X.; Wei, A.; Sha, M.; Fu, J.; Liu, Y.; Zhong, J.; Sun, X. Blue Energy Collection toward All-Hours Self-Powered Chemical Energy Conversion. *Adv. Energy Mater.* **2020**, *10*, 2001041.
(43) Jiang, D.; Ouyang, H.; Shi, B.; Zou, Y.; Tan, P.; Qu, X.; Chao, S.; Xi, Y.; Zhao, C.; Fan, Y.; Li, Z. A Wearable Noncontact Free-Rotating Hybrid Nanogenerator for Self-Powered Electronics. *InfoMat* **2020**, *2*, 1911−1200.
(44) Ouyang, H.; Jiang, D.; Fan, Y.; Wang, Z. L.; Li, Z. Self-Powered Technology for Next-Generation Biosensor. *Sci. Bull.* **2021**, *66*, 1709−1712.
(45) Jiang, J.; Guan, Q.; Liu, Y.; Sun, X.; Wen, Z. Abrasion and Fracture Self-healable Triboelectric Nanogenerator with Ultrahigh Stretchability and Long-term Durability. *Adv. Funct. Mater.* **2021**, *31*, 2105380.
(46) Yang, Y.; Xu, L.; Jiang, D.; Chen, B. Z.; Luo, R.; Liu, Z.; Qu, X.; Wang, C.; Shan, Y.; Cui, Y.; Zheng, H.; Wang, Z.; Wang, Z. L.; Guo, X. D.; Li, Z. Self-Powered Controllable Transdermal Drug Delivery System. *Adv. Funct. Mater.* **2021**, *31*, 2104092.
(47) Qu, X.; Ma, X.; Shi, B.; Li, H.; Zheng, L.; Wang, C.; Liu, Z.; Fan, Y.; Chen, X.; Li, Z.; Wang, Z. L. Refreshable Braille Display System Based on Triboelectric Nanogenerator and Dielectric Elastomer. *Adv. Funct. Mater.* **2021**, *31*, 2006612.
(48) Xiao, M.; Wang, L.; Ji, F.; Shi, F. Converting Chemical Energy to Electricity through A Three-Jaw Mini-Generator Driven by the

https://doi.org/10.1021/acsami.2c04651
ACS Appl. Mater. Interfaces 2022, 14, 22206−22215

Decomposition of Hydrogen Peroxide. *ACS Appl. Mater. Interfaces* **2016**, *8*, 11403−11411.
(49) Niu, S.; Liu, Y.; Chen, X.; Wang, S.; Zhou, Y. S.; Lin, L.; Xie, Y.; Wang, Z. L. Theory of freestanding triboelectriclayer-based nanogenerators. *Nano Energy* **2015**, *12*, 760−774.

https://doi.org/10.1021/acsami.2c04651
ACS Appl. Mater. Interfaces 2022, 14, 22206−22215